JOURNAL OF THERMOPHYSICS AND HEAT TRANSFER
Vol. 13, No. 1, January–March 1999

Viscous Shock-Layer Simulation of Airflow past Ablating Blunt Body with Carbon Surface

Sergey V. Zhluktov* and Takashi Abe†
Institute of Space and Astronautical Science, Sagamihara City, Kanagawa 229, Japan

A kinetic model for air–carbon surface interaction is suggested. The model is based on the langmuir approach to the kinetics of catalytic reactions. It yields a reasonable agreement with published experimental data on graphite oxidation. A viscous shock-layer code has been developed to simulate hypersonic flows of the 19-species mixture containing air and carbon products. Numerical analysis of ablation and strong ionization processes is carried out with different ablation and ionization models. Calculations show that 1) the maximal drop of the heat flux because of ablation, compared with that obtained for the fully catalytic (chemical-equilibrium) wall in the 11-species air, is within 26% under the conditions discussed; 2) mass loss rate strongly depends on the adsorption type (mobile/immobile); 3) ionization model may have a substantial influence on the shock thickness in the case of re-entry with a hyperbolic velocity; and 4) the effect of the wall catalycity with respect to charged particles on the heating rate is small.

Nomenclature

B = number of active cites per square meter
C_i = mass fraction of species i
$(C - i)$ = adatom i, O or N
C_{pi} = specific heat of species i
D_{ik} = binary diffusion coefficients
H = full enthalpy
h = Planck's constant
h_i = specific enthalpy of species i
J_i = diffusion flux of species i
J_q = heat flux
K_i = equilibrium constant for reaction i
k = Boltzmann's constant
k_{fi} = rate constant of the forward heterogeneous reaction i
k_{ri} = rate constant of the backward heterogeneous reaction i
$\dot{m}$ = mass loss rate
m_i = mass or molar mass of species i
$\dot{m}_i$ = mass production rate of species i
m_1–m_{10} = third particles in different reactions of dissociation
P = pressure
q_r = radiation flux
R_A = universal gas constant
R_n = nose radius
r_i = rate of heterogeneous reaction i
T = temperature
T_{ai} = characteristic activation temperature for reaction i
T_{Di} = characteristic temperature of dissociation of molecular species i
T_{di} = characteristic temperature of atomic desorption, i = O or N
V_∞ = freestream velocity
X_i = molar fraction of species i
ε = blackness of the body surface
ε_i = factor in the ith forward or backward heterogeneous rate constant
Θ^0 = free surface concentration
Θ_i = surface concentration of atomic species i, i = O or N
λ = heat conductivity
μ = viscosity
ρ = density
σ = Stefan–Boltzmann's constant

Subscripts
n = normal projection of vector
w = body surface

Superscripts
gas = gas phase
int = internal degrees of freedom
sol = solid body
tr = translational degrees of freedom

Introduction

THE MUSES-C program is a sample return mission from an asteroid.[1] In the program, a return capsule directly reenters the Earth's atmosphere at superorbital speed. On the carbonaceous surface of the ablation-type heat shield of the capsule, a variety of chemical processes proceed. Understanding their details is important for the correct prediction of heat fluxes and mass loss rates.

A vast literature exists on the carbon surface chemistry. The first experiments were carried out more than one hundred years ago. The first theoretical findings belong to Langmuir. Unfortunately, no universal kinetic model of the carbon surface oxidation was created for this period. The existing models are too crude and too empirical.[2,3] Moreover, there is no common opinion among investigators about what are the main processes on the carbon surface. In Ref. 4, controlling mechanisms are discussed. Often, two different kinds of active sites are assumed.[5–7] In Ref. 7 it is pointed out that the second-type (not pure-graphite) sites are on a hydrocarbon material that is left in the production process. In the present study, we consider graphite-type surfaces with only pure-graphite active sites; otherwise it would be necessary to introduce hydrogen-containing

Received June 25, 1997; revision received June 1, 1998; accepted for publication July 30, 1998. Copyright © 1998 by the American Institute of Aeronautics and Astronautics, Inc. All rights reserved.

*Visiting Researcher, on leave from the Russian Academy of Sciences, Institute for Computer-Aided Design, 2-d Brestskaya 19/18, Moscow 123056, Russia, Major Researcher.

†Professor, Division of Space Transportation, Senior Member AIAA.

species into the gas-phase kinetic model of the shock layer. Another problem is the porosity of real graphites and, particularly, charcoals and porous diffusion effects. According to Ref. 8, the effects may change the observed order of the surface reaction. In the present study the effects are also neglected.

Different kinetic schemes are suggested by different authors. Sometimes, one can see a contradiction between researchers. For example, Ref. 9 contradicts Refs. 10 and 11 about what is the main mechanism of CO_2 formation. In the present study, the viewpoint of Ref. 9 has been accepted. Note that a reasonable way to bypass the discussion about governing processes and intermediate steps is to postulate full equilibrium on the carbon surface (see, e.g., Ref. 12), i.e., to assume that the regime is always diffusion controlled. In doing so, chemical composition at the wall is calculated as an equilibrium one at a given pressure and temperature, and the mass conservation equations are integrated with the first-kind boundary conditions on the body surface. In the case of a chemically inert surface, this corresponds to an assumption of the full catalycity.

The approach used in the present work is similar in a sense to approaches implemented to the heterogeneous recombination of partly dissociated air on an SiO_2 surface,[13,14] which in turn, developed the original ideas of Langmuir (see, e.g., Ref. 15). On some points our approach is close to that of Ref. 11. Meanwhile, it is more crude than Ong's approach,[11] in accordance with initial motivation to create a robust and more or less universal model.

A viscous shock-layer (VSL) code has been developed for the simulation of chemical and thermal nonequilibrium airflows past smooth blunted axisymmetric bodies.[16–18] The algorithm is used in the present study to investigate effects of blowout and strong ionization on the flowfield around the MUSES-C re-entry capsule. The capsule is a 45-deg, spherically blunted cone with a nose radius of 0.2 m and a base diameter of 0.4 m. The following freestream conditions are considered: V_∞ = 11,500 m/s, $\rho_\infty = 1.6310^{-4}$ kg/m^3, and T_∞ = 233.3 K. According to the preliminary analysis,[19] this point of the trajectory corresponds to maximal heat loads on the capsule.

Kinetic Model for Heterogeneous Processes

The following kinetic model is suggested:

$$
\begin{aligned}
&1.\ \ \mathrm{O} + (\mathrm{C}) \Leftrightarrow (\mathrm{C}-\mathrm{O})\\
&2.\ \ \mathrm{O_2} + 2(\mathrm{C}) \Leftrightarrow 2(\mathrm{C}-\mathrm{O})\\
&3.\ \ \mathrm{O_2} + (\mathrm{C}) \Leftrightarrow (\mathrm{C}-\mathrm{O}) + \mathrm{O}\\
&4.\ \ \mathrm{O_2} + (\mathrm{C}) \Leftrightarrow (\mathrm{C}-\mathrm{O}) + \mathrm{CO}\\
&5.\ \ (\mathrm{C}-\mathrm{O}) \Leftrightarrow \mathrm{CO} + (\mathrm{C})\\
&6.\ \ \mathrm{O} + (\mathrm{C}-\mathrm{O}) \Leftrightarrow \mathrm{CO_2} + (\mathrm{C})\\
&7.\ \ 2(\mathrm{C}-\mathrm{O}) \Leftrightarrow \mathrm{CO_2} + 2(\mathrm{C})\\
&8.\ \ (\mathrm{C}) \Leftrightarrow \mathrm{C} + (\mathrm{C})\\
&9.\ \ 2(\mathrm{C})\ \mathrm{p} \Leftrightarrow \mathrm{C_2} + 2(\mathrm{C})\\
&10.\ \ 3(\mathrm{C}) \Leftrightarrow \mathrm{C_3} + 3(\mathrm{C})\\
&11.\ \ \mathrm{N} + (\mathrm{C}) \Leftrightarrow (\mathrm{C}-\mathrm{N})\\
&12.\ \ (\mathrm{C}-\mathrm{N}) + \mathrm{N} \Leftrightarrow \mathrm{N_2} + (\mathrm{C})
\end{aligned}
\qquad (1)
$$

Chemisorption of molecular species is not taken into account. The model contains the reactions mentioned in literature as being important. Corresponding reaction rates are as follows:

$$
\begin{aligned}
r_1 &= k_{f1}(PX_\mathrm{O}\Theta^0 - \Theta_\mathrm{O}/K_1)\\
r_2 &= k_{r2}[K_2 PX_{\mathrm{O}_2}(\Theta^0)^2 - (\Theta_\mathrm{O})^2]\\
r_3 &= k_{f3}(PX_{\mathrm{O}_2}\Theta^0 - PX_\mathrm{O}\Theta_\mathrm{O}/K_3)\\
r_4 &= k_{f4}(PX_{\mathrm{CO}_2}\Theta^0 - PX_\mathrm{CO}\Theta_\mathrm{O}/K_4)\\
r_5 &= k_{f5}(\Theta_\mathrm{O} - PX_\mathrm{CO}\Theta^0/K_5)\\
r_6 &= k_{f6}(PX_\mathrm{O}\Theta_\mathrm{O} - PX_{\mathrm{CO}_2}\Theta^0/K_6)\\
r_7 &= k_{f7}[(\Theta_\mathrm{O})^2 - PX_{\mathrm{CO}_2}(\Theta^0)^2/K_7]\\
r_8 &= k_{r8}\Theta^0(K_8 - PX_\mathrm{C})\\
r_9 &= k_{r9}(\Theta^0)^2(K_9 - PX_{\mathrm{C}_2})\\
r_{10} &= k_{r10}(\Theta^0)^3(K_{10} - PX_{\mathrm{C}_3})\\
r_{11} &= k_{f11}(PX_\mathrm{N}\Theta^0 - \Theta_\mathrm{N}/K_{11})\\
r_{12} &= k_{r12}(K_{12}PX_\mathrm{N}\Theta_\mathrm{N} - PX_{\mathrm{N}_2}\Theta^0)
\end{aligned}
\qquad (2)
$$

It is assumed that two possibilities exist for K_1 and K_{11}. The first is a mobile adsorption. In this case

$$
\frac{1}{K_i} = B\frac{kT}{P_0}\left(\frac{2\pi m_i kT}{h^2}\right)^{1/2} e^{-T_{di}/T}, \quad \text{atm} \qquad (3)
$$

The second is immobile adsorption. In that case

$$
\frac{1}{K_i} = \frac{kT}{P_0}\left(\frac{2\pi m_i kT}{h^2}\right)^{3/2} e^{-T_{di}/T}, \quad \text{atm} \qquad (4)
$$

where i = 1 or 11, $m_i = m_\mathrm{O}$ or m_N; $P_0 = 1.01325 \times 10^5$ Pa; and $B = 3.5 \times 10^{19}$ m^{-2}.[8] It is assumed here that the partition function corresponding to the normal (to the surface) vibrations of adatom is unity.

The important point is that equilibrium constants $K_1 \sim K_{12}$ are not independent. On the contrary, they are related via gas-phase equilibrium constants of corresponding dissociation processes:

$$
\begin{aligned}
K_2 &= (K_1)^2 K_{\mathrm{O}_2}\\
K_3 &= K_1 K_{\mathrm{O}_2}\\
K_4 &= K_1 K_{\mathrm{CO}_2}\\
K_5 &= K_8/(K_1 K_\mathrm{CO})\\
K_6 &= K_8/(K_1 K_\mathrm{CO} K_{\mathrm{CO}_2})\\
K_7 &= K_8/[(K_1)^2 K_\mathrm{CO} K_{\mathrm{CO}_2}]\\
K_9 &= (K_8)^2/K_{\mathrm{C}_2}\\
K_{10} &= (K_8)^3/(K_{\mathrm{C}_2} K_{\mathrm{C}_3})\\
K_{12} &= 1/(K_{11} K_{\mathrm{N}_2})
\end{aligned}
\qquad (5)
$$

Knowing equilibrium constants and specifying rate constants either for the forward or backward reactions, we shall get a complete set of heterogeneous kinetic data. Recom-

mended expressions for the necessary forward/backward reaction rate constants are as follows:

$$\begin{aligned}
k_{f1} &= \varepsilon_1 f_O \\
k_{r2} &= \varepsilon_2 B(kT/h)e^{-T_{a2}/T} \\
k_{f3} &= \varepsilon_3 f_{O_2} e^{-T_{a3}/T} \\
k_{f4} &= \varepsilon_4 f_{CO_2} \\
k_{f5} &= \varepsilon_5 B(kT/h)e^{-T_{a5}/T} \\
k_{f6} &= \varepsilon_6 f_O e^{-T_{a6}/T} \\
k_{f7} &= \varepsilon_7 B(kT/h)e^{-T_{a7}/T} \\
k_{r8} &= \varepsilon_8 f_C \\
k_{r9} &= \varepsilon_9 f_{C_2} \\
k_{r10} &= \varepsilon_{10} f_{C_3} \\
k_{f11} &= \varepsilon_{11} f_N \\
k_{r12} &= \varepsilon_{12} f_{N_2} e^{-T_{a12}/T}
\end{aligned} \tag{6}$$

where

$$f_i = P_0/\sqrt{2\pi m_i kT} \tag{7}$$

The recommended values of the parameters are $\varepsilon_1 = 1$, $\varepsilon_2 = 8 \times 10^{-4}$, $\varepsilon_3 = 1$, $\varepsilon_4 = 0.9$, $\varepsilon_5 = 0.1$, $\varepsilon_6 = 0.8$, $\varepsilon_7 = 1$, $\varepsilon_8 = 0.24$, $\varepsilon_9 = 0.5$, $\varepsilon_{10} = 0.023$, $\varepsilon_{11} = 1$, $\varepsilon_{12} = 1$; and $T_{d1} = 45{,}000$, $T_{d11} = 36{,}600$,

$$\begin{aligned}
T_{a2} &= 2T_{d1} - T_{DO_2} \\
T_{a3} &= T_{DO_2} - T_{d1} \\
T_{a12} &= T_{DN_2} - T_{d11}
\end{aligned} \tag{8}$$

$T_{a5} = 40{,}000$, 34,000, or 27,000; $T_{a6} = 2000$ or 1000; and $T_{a7} = 40{,}000$, 34,000, or 13,700. Coefficients $\varepsilon_8 \sim \varepsilon_{10}$ have been taken from Ref. 20. There are few expressions for K_8 in literature.[12,20,21] Values of Baker[21] and Scala and Gilbert[12] are very close to each other, whereas Blottner's[20] K_8 may be 2.5 times higher. To estimate the maximal effect of ablation, Blottner's expression for K_8 is used in the present study; K_9 and K_{10} are obtained from Eqs. (5).

Now let us write the rates of species production on the surface:

$$\begin{aligned}
\dot{m}_O/m_O &= -r_1 + r_3 - r_6 \\
\dot{m}_{CO}/m_{CO} &= r_4 + r_5 \\
\dot{m}_{CO_2}/m_{CO_2} &= -r_4 + r_6 + r_7 \\
\dot{m}_C/m_C &= r_8 \\
\dot{m}_{C_2}/m_{C_2} &= r_9 \\
\dot{m}_{C_3}/m_{C_3} &= r_{10} \\
\dot{m}_{NO}/m_{NO} &= 0 \\
\dot{m}_{CN}/m_{CN} &= 0 \\
\dot{m}_N/m_N &= -r_{11} - r_{12} \\
\dot{m}_{O_2}/m_{O_2} &= -r_2 - r_3 \\
\dot{m}_{N_2}/m_{N_2} &= r_{12}
\end{aligned} \tag{9}$$

For a stationary regime we have

$$\begin{aligned}
\dot{m}_{(C-O)}/m_O &= r_1 + 2r_2 + r_3 + r_4 - r_5 - r_6 - 2r_7 = 0 \\
\dot{m}_{(C-N)}/m_N &= r_{11} - r_{12} = 0
\end{aligned} \tag{10}$$

Using these expressions, we get

$$\dot{m} = \sum \dot{m}_i = m_C(r_5 + r_6 + r_7 + r_8 + 2r_9 + 3r_{10}) \tag{11}$$

The solution of Eqs. (10) together with the apparent following relationship:

$$\Theta_O + \Theta_N + \Theta^0 = 1 \tag{12}$$

yields Θ_O, Θ_N, and Θ^0 values. Substituting these values into r_i and specifying fractions of the gas species, pressure, and temperature, we obtain the necessary mass production rates as well as the mass loss rate.

Discussion of the Model

Numerous experimental data on carbon oxidation are published, as well as kinetic models and expressions describing these data. Differences in the corresponding mass loss rates may be more than one order. The reason for the discrepancy is the difference in the carbons/graphites tested. Initial calculations with the model discussed showed that when we fit the model to one set of experimental data we obtain disagreements with other experiments. This is why it was decided to do a rough fitting to the available experimental data with the recommendation of a reasonable range of the model parameters.

Calculations showed that it is possible to recommend fixed values of ε_i. Note that, in general, ε_i are at most power functions of temperature and contain information about activation complexes, sticking coefficients, and steric factors. The recommended values of T_{di} and T_{ai} have been chosen after great a deal of calculations with different input parameters. It was found that the best qualitative (nonmonotone behavior of the plots) and quantitative agreement with experiments is achieved when kT_{d1} is close to the energy of a single C–O bond.

It is necessary to note that there are not many data on carbon–nitrogen interactions. According to Ref. 22, the primary product of the interaction is C_2N_2, and its amount is negligible. Therefore, corresponding reactions are not taken into account. As far as we know, there is no published information on the adsorption–desorption, Eley–Rideal, and Langmuir–Hinshelwood reactions for nitrogen interacting with a carbonaceous surface. Therefore, it was assumed that only adsorption–desorption of atomic nitrogen and Eley–Rideal reactions occur, and the value of kT_{d11} should be around the energy of the single C–N bond.

Actually, few possibilities exist for T_{ai}, $i = 5$, 6, and 7. In Figs. 1–3 one can see calculations with $T_{a5} = T_{a7} = 40{,}000$ K and $T_{a6} = 2000$ K (black squares); with $T_{a5} = T_{a7} = 34{,}000$ K and $T_{a6} = 1000$ K (clear squares); and calculations with $T_{a5} = 27{,}000$ K and $T_{a7} = 13{,}700$ K (crosses). The first two cases correspond to mobile adsorption, with the third case corresponding to immobile adsorption. In the third case we get a good agreement with the data of Ref. 23 for high pressures (black line in Fig. 1). In the first case we have good agreement with Rosner and Allendorf's data[24] for pyrolytic graphite at low pressures (solid lines in Fig. 2 for pure O_2 and O, respectively). In the second case we shift toward their data for isotropic graphite (dashed lines in Fig. 2). Note that the values of $T_{a5} = 27{,}000$ K and $T_{a7} = 13{,}700$ K, and the assumption of immobile adsorption are close to the recommendations of Ref. 11 for high-pressure processes. Note also that the value of $T_{a5} = 40{,}000$ K corresponds to the energy of the single C–C bond. This coincides with the recommendation of Blyholder and Eyring[8] for reaction 5 on the basal plane of pyrolytic graphite at

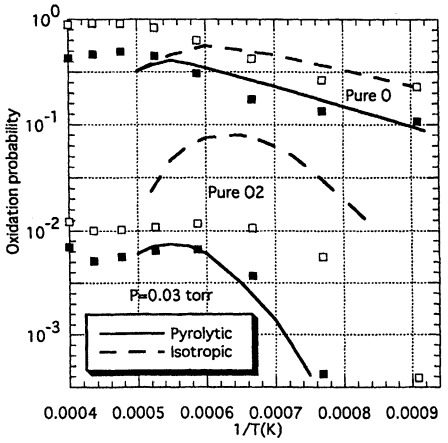

Fig. 1 Effect of activation energies and adsorption type on the mass loss rate (high pressures).

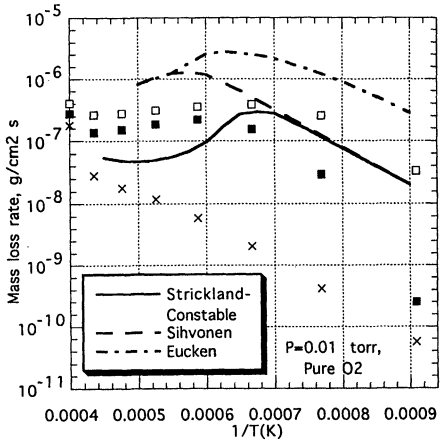

Fig. 2 Effect of activation energies on the oxidation probability (low pressures).

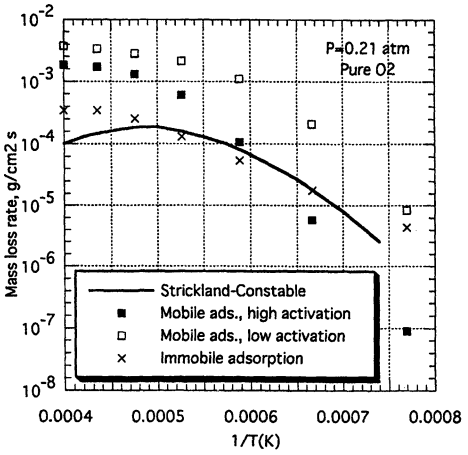

Fig. 3 Effect of activation energies and adsorption type on the mass loss rate (low pressures).

low pressures. In Fig. 3, the calculations are plotted together with the experimental data of different authors (solid, dashed, and dash–dotted lines taken from Ref. 4). The reaction products were removed in the experiments discussed; therefore, we assume in our calculations that the corresponding gas is pure, i.e., contains no admixtures.

It seems that kinetics of the heterogeneous processes at high pressures differ from those at low pressures. Of course, the model discussed cannot switch automatically from one kinetic to another. Actual kinetics include the adsorption–desorption of molecules, the migration of the adsorbed particles to edge carbon atoms or to impurities, and different activation mechanisms at single- and double-bonded edge carbon atoms and different impurities. Therefore, the suggested model should be considered as an alternative one: it is finer than most models given in literature because it contains more reactions. At the same time it remains rather rough because it does not take into account many intermediate processes.

Governing Equations and Boundary Conditions

Viscous shock layer (VSL) equations result from Navier–Stokes equations by neglecting terms less than $\mathcal{O}(\mathrm{Re}^{-1/2})$ in the scale of the boundary-layer thickness. The VSL model allows for upstream propagation of sonic disturbances in subsonic regions and enables one to calculate the shock shape. The model was discussed in detail in Refs. 17 and 18.

A one-temperature model is implemented in the work. Our kinetic system of gas-phase processes includes 40 reactions. The reactions and corresponding references to the reaction rates are listed next:

1. $O_2 + m_1 \Leftrightarrow 2O + m_1$, Ref. 20
2. $N_2 + m_2 \Leftrightarrow 2N + m_2$, Ref. 20

   $N_2 + N \Leftrightarrow 3N$, Ref. 20
3. $NO + m_3 \Leftrightarrow N + O + m_3$, Ref. 20
4. $O + N_2 \Leftrightarrow N + NO$, Ref. 20
5. $O + NO \Leftrightarrow N + O_2$, Ref. 20
6. $O + N \Leftrightarrow NO^+ + E$, Ref. 20
7. $2O \Leftrightarrow O_2^+ + E$, Ref. 25
8. $2N \Leftrightarrow N_2^+ + E$, Ref. 25
9. $O + O_2^+ \Leftrightarrow O_2 + O^+$, Ref. 25
10. $N_2 + N^+ \Leftrightarrow N + N_2^+$, Ref. 25
11. $O + NO^+ \Leftrightarrow NO + O^+$, Ref. 25
12. $N_2 + O^+ \Leftrightarrow O + N_2^+$, Ref. 25
13. $O_2 + NO^+ \Leftrightarrow NO + O_2^+$, Ref. 25
14. $N + NO^+ \Leftrightarrow NO + N^+$, Ref. 25
15. $O + NO^+ \Leftrightarrow O_2 + N^+$, Ref. 25
16. $CO_2 + m_5 \Leftrightarrow CO + O + m_5$, Ref. 20
17. $CO + m_6 \Leftrightarrow C + O + m_6$, Ref. 20
18. $C_2 + m_7 \Leftrightarrow 2C + m_7$, Ref. 20
19. $C_3 + m_8 \Leftrightarrow C + C_2 + m_8$, Ref. 20
20. $CN + m_9 \Leftrightarrow C + N + m_9$, Ref. 20
21. $N_2 + C \Leftrightarrow CN + N$, Ref. 20
22. $CO + N \Leftrightarrow CN + O$, Ref. 20
23. $CO_2 + N \Leftrightarrow CN + O_2$, Ref. 20
24. $N_2 + CO \Leftrightarrow CN + NO$, Ref. 20
25. $CO + NO \Leftrightarrow CO_2 + N$, Ref. 20
26. $CO_2 + O \Leftrightarrow CO + O_2$, Ref. 20
27. $2CO \Leftrightarrow CO_2 + C$, Ref. 20
28. $CO + O \Leftrightarrow O_2 + C$, Ref. 20
29. $CO + N \Leftrightarrow C + NO$, Ref. 20

30. $CN + O \Leftrightarrow C + NO$, Ref. 20
31. $CO + C \Leftrightarrow C_2 + O$, Ref. 20
32. $C_2 + CO \Leftrightarrow C_3 + O$, Ref. 20
33. $C_3 + C \Leftrightarrow 2C_2$, Ref. 20
34. $O_2 + C^+ \Leftrightarrow O_2^+ + C$, Ref. 26
35. $Co + C^+ \Leftrightarrow CO + C$, Ref. 26
36. $NO + C^+ \Leftrightarrow NO^+ + C$, Ref. 26
37. $C + O \Leftrightarrow CO^+ + E^-$, Ref. 26
38. $O + E^- \Leftrightarrow O^+ + 2E^-$, Ref. 25
39. $N + E^- \Leftrightarrow N^+ + 2E^-$, Ref. 25
40. $C + E^- \Leftrightarrow C^+ + 2E^-$, Ref. 26 (13)

The reactions that were excluded from the systems of Blottner[20] ($2CO \Leftrightarrow C_2 + O_2$) and Kang[25] ($O_2 + N_2 \Leftrightarrow NO + NO^+ + E^-$; $NO + m_{10} \Leftrightarrow NO^+ + E^- + m_{10}$) are relatively slow. An important subject should be discussed here. As we see, equilibrium constants for sublimation processes depend on each other and on gas-phase equilibrium constants. Unfortunately, in literature we find different data on heterogeneous and homogeneous equilibrium constants that do not satisfy Eqs. (5). Moreover, published gas-phase reactions themselves are often incompatible in terms of equilibrium constants, and may lead to difficulties in calculating near-equilibrium flows. The incompatibility between homogeneous and heterogeneous equilibrium constants may lead to incorrect predictions of heating and mass-loss rates. After analysis of different reaction rate systems, we assume that the rate constant of the backward-reaction $C_3 + m_8 \Leftrightarrow C_2 + C + m_8$, recommended by Blottner, is wrong. We corrected it using Scala and Gilbert's[12] expression for an equilibrium constant of the process $C_3 \Leftrightarrow 3C$. In doing so, we eliminated the most prominent incompatibility in the implemented reaction system, whereas minor disagreements between equilibrium constants still exist, and a special study is necessary to compile a consistent rate system for future work.

Stefan–Maxwell relationships are used to describe multicomponent diffusion in the shock layer. Pressure-diffusion, thermodiffusion, and radiation are not taken into account. It is assumed that the conditions of quasineutrality and the absence of electric current hold from the shock until the body surface. To calculate viscosity and transport thermal conductivity of the mixture, the approach of Ref. 27 is used. Full heat conductivity of the mixture is calculated as follows:

$$\lambda = \lambda^{tr} + \lambda^{int} \tag{14}$$

$$\lambda^{int} = \rho \sum_{i=1}^{N} D_i \frac{C_i}{m_i} (C_{pi} - 2.5R_A)$$
$$\frac{1}{D_i} = \sum_{k=1}^{N} \frac{X_k}{D_{ik}} \tag{15}$$

It is assumed that all of the molecules are in the ground electronic state, and their vibrational energies are calculated as for harmonic oscillator cutoff at the dissociation limit. Electronic energies of atoms are calculated using curve fits from Ref. 28. We take the electronic energy of C equal to that of N^+ and the electronic energy of C^+ equal to zero.

Rankine–Hugoniot shock-slip relationships are used as boundary conditions on the shock wave.[16,17] On the body surface we specify a no-slip condition for the tangent momentum equation. For the charged particles we consider two possibilities: their production rates are zero at the wall or their fractions correspond to the equilibrium composition at the wall temperature and pressure. The mass production rates of neutral species and the total mass loss rate are specified explicitly within the kinetic model discussed.

In the case of equilibrium ablation (19-species mixture) or fully catalytic surface (11-species air), the equilibrium composition of neutral species on the wall is calculated using values of the elements O_2 and C (for ablation). The values of the mass fractions and diffusion fluxes of these elements on the body surface are obtained after integration of the corresponding (homogeneous) mass-conservation equations. The diffusion flux of the element C on the wall is used to calculate the mass loss rate.

In general, energy balancing on the ablating body surface is

$$-J_{qn}^{gas} + q_{rn} - \sigma\varepsilon T_w^4 = -J_{qn}^{sol} + \dot{m}(H_w^{gas} - H_w^{sol}) \tag{16}$$

where

$$J_q = -\lambda \nabla T + \sum_{i=1}^{N} J_i h_i \tag{17}$$

The heat flux into the body can be roughly taken as quasi-stationary

$$-J_{qn}^{sol} \approx \dot{m} C_p^{sol} T_w \tag{18}$$

Then, neglecting q_{rn}, and substituting $-J_{qn}^{sol}$ and $H_w^{sol} = C_p^{sol} T_w$ into Eq. (16), we have

$$-J_{qn}^{gas} - \sigma\varepsilon T_w^4 = \dot{m} H_w^{gas} \tag{19}$$

Thus, we have a few of the mixed boundary conditions on the body and shock wave for every species mass conservation equation, for the energy conservation equation, as well as for the tangent momentum equation. Therefore, a sweep method should be used to integrate the equations across the shock layer.

Numerical Method

Steady VSL equations have elliptic properties because of the streamwise component of pressure gradient and the shock-wave slope. This is why the marching solution of the equations is not correct, and some relaxation procedures should be implemented. To solve the problem, the method of global iterations (GI)[29] is used in the present work. The method reduces the integration of the VSL system to several marching passes (GIs) along the body, the initial boundary-value problem being well posed for each GI (in the absence of reverse flows).

Richardson's (implicit two-order) scheme[29] is used in a streamwise direction. Petukhov's (four-order) scheme[29] is used in the normal direction for integration of the tangent momentum, energy, and species mass conservation equations. The coupled continuity and normal momentum equations are solved using a finite difference method that generalizes the Petukhov approach for sets of hyperbolic equations. Symmetric approximation is implemented for the calculation of the pressure streamwise derivative and the shock slope. No smoothing procedure is employed.

A spherically blunted cone is a body with a broken curvature. This curvature discontinuity may significantly affect the derivatives of the flow characteristics, such as pressure and shock standoff distance, with respect to the streamwise coordinate. To avoid peculiarities in these derivatives and to keep the second-order approximation, the exact relationships for the derivatives at the point of the sphere–cone junction[18,29] are used. References 18 and 29 contain more details on the numerical approach discussed.

At each step along the body, the VSL system is solved iteratively by Newton's method. An adaptive grid (automatically condensing in the regions with large gradients, e.g., near the

wall and behind the shock, and large second derivatives) is used in the normal direction. The amount of GIs necessary for the solution to converge with 1% accuracy is comparable with the amount of grid nodes in the streamwise direction. After checking grid convergence, the uniform grid consisting of 25 intervals along the sphere–cone axis of symmetry has been chosen as rational for systematic calculations. From these 25 intervals, 10 intervals fall onto the spherical part of the body, another 10 correspond to the conic part, and five nodes fall behind the theoretical body edge. These extra nodes exclude the influence of the soft (supersonic) boundary conditions implemented at the downstream end of the computational region and enable us to obtain flow characteristics at the body edge as if the cone were infinite. Of course, this is mainly of academic interest because the real flow expands significantly around the body edge, which has a finite curvature. About 90 nodes are used across the shock layer. Note that the working amount of grid nodes is four times more, because both Richardson's and Petukhov's schemes assume a calculation of the flow characteristics in the middle of every interval.

The codes have been implemented previously for calculations of thermochemical nonequilibrium airflows around analytic axisymmetric blunted bodies[16] and spherically blunted cones,[17] as well as for calculations of chemical nonequilibrium thermal equilibrium flows of air around a body consisting of two spherical and two conic segments.[18] The code has been compared with the code of Ref. 19, first in calculations of airflows, and then in calculations of the flows of the 19-species mixture. Despite the differences between the codes in numerical approaches and models for transport processes and heterogeneous kinetics, the comparisons have shown a satisfactory agreement in the flow characteristics.

Results and Discussion

In Fig. 4, temperature profiles across the shock layer are shown in the stagnation point, in the point of sphere-cone junction, and in the point corresponding to the edge of MUSES-C capsule. The calculations are done under the condition of equilibrium ablation. In Figs. 5 and 6, profiles of N and N^+ molar fractions are represented (notations are the same). From the profiles one can see the dynamics of deionization along the body. It is important to discuss the effect of the shock-slip boundary conditions [see Eq. (34) in Ref. 17]. Their implementation makes fractions of atoms and ions behind the shock finite, because the diffusion fluxes are large in the relaxation region. This leads to a substantial drop in temperature in com-

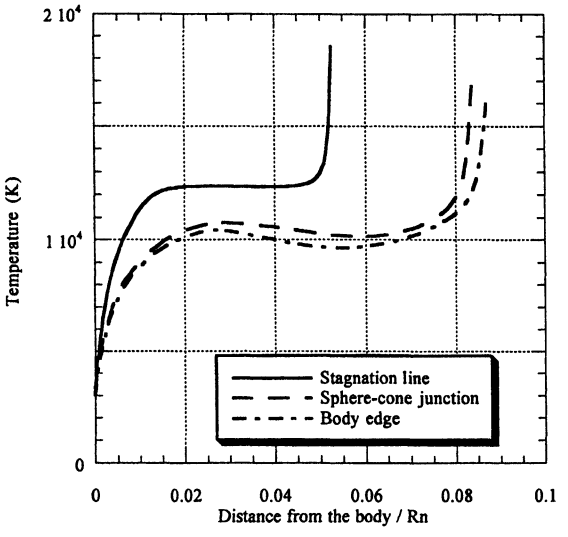

Fig. 4 Temperature profiles across the shock layer (equilibrium ablation).

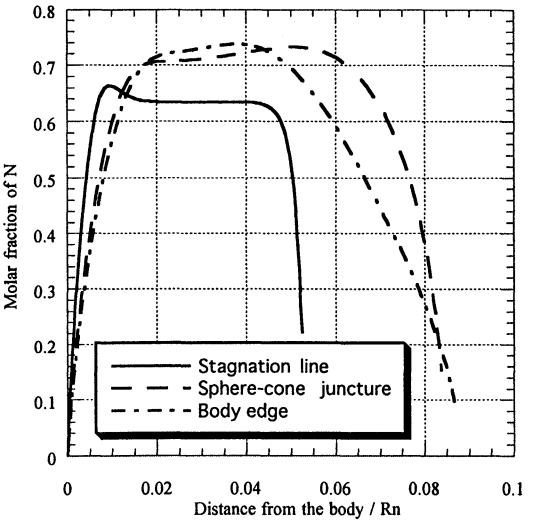

Fig. 5 Profiles of N molar fraction across the shock layer (equilibrium ablation).

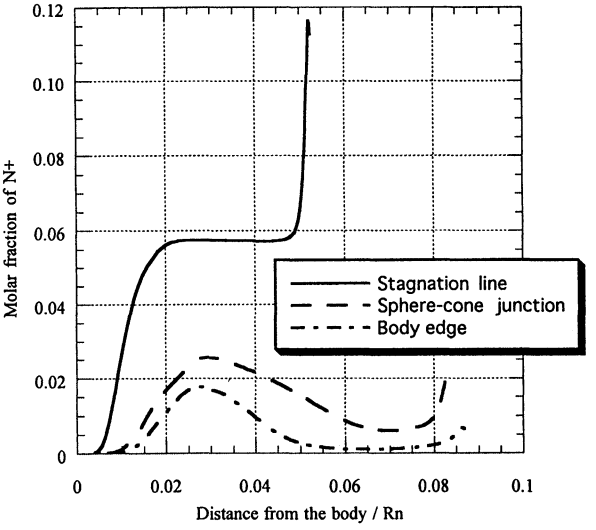

Fig. 6 Profiles of N^+ molar fraction across the shock layer (equilibruim ablation).

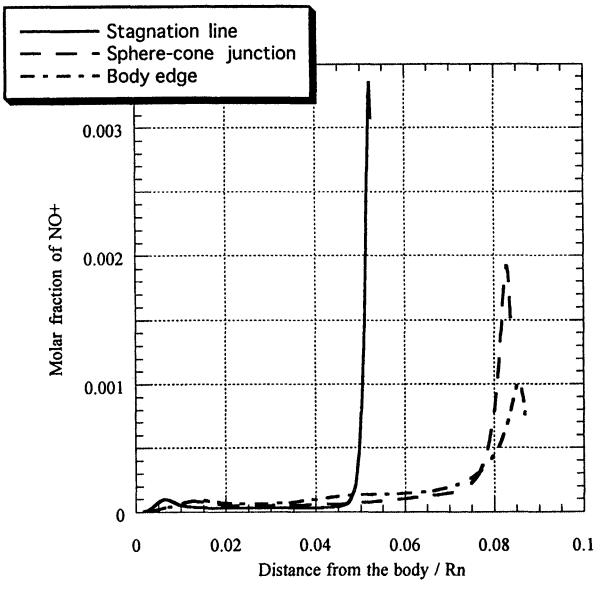

Fig. 7 Profiles of NO molar fraction across the shock layer (equilibrium ablation).

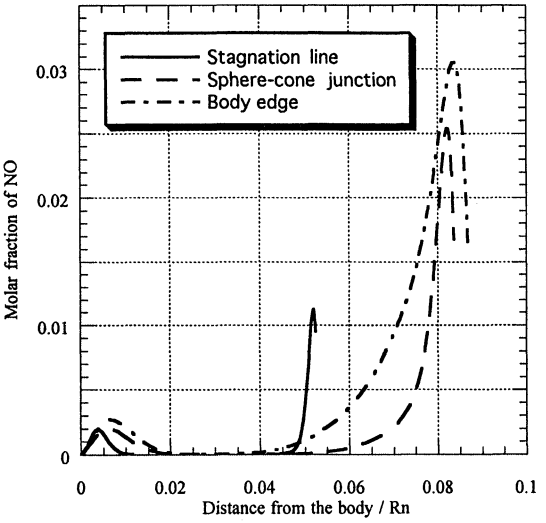

Fig. 8 Profiles of NO^+ molar fraction across the shock layer (equilibrium ablation).

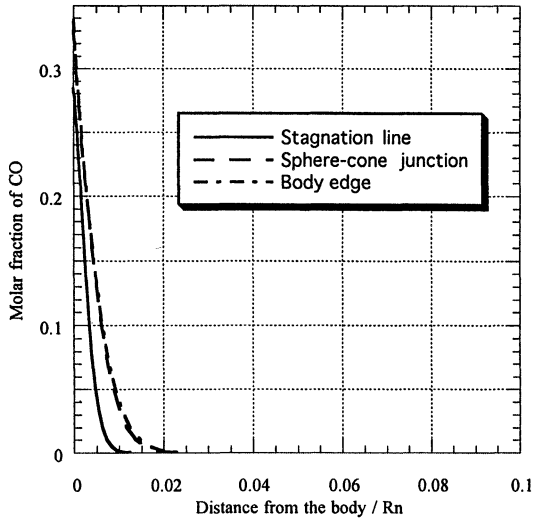

Fig. 9 Profiles of CO molar fraction across the shock layer (equilibrium ablation).

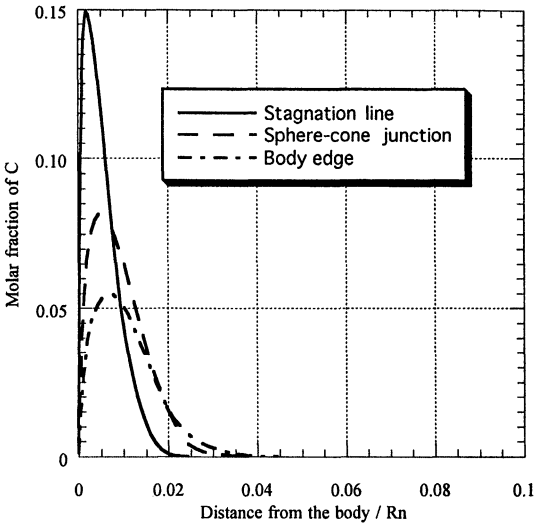

Fig. 10 Profiles of C molar fraction across the shock layer (equilibrium ablation).

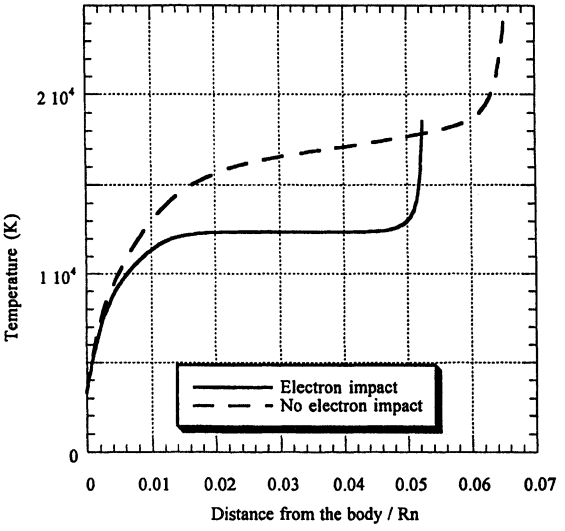

Fig. 11 Effect of ionization model on temperature (equilibrium ablation, stagnation line).

parison with ordinary Rankine–Hugoniot calculations. Profiles of X_{NO}, $X_{NO^+}X_{CO}$, and X_C are shown in Figs. 7–10, respectively.

It was important for us to estimate the effect of the reactions of ionization by electron impact on the MUSES-C re-entry environment. In Fig. 11 one can see the stagnation-point temperature profiles obtained with and without the reactions for the case of equilibrium ablation. Corresponding profiles of X_E, X_{N^+}, and X_{O^+} are given in Fig. 12. Apparently, taking the electon-impact ionization into account leads to ionization equilibrium in a major portion of the shock layer under the conditions discussed (one can see that fractions of ions grow and actually follow the temperature). Consequently, the temperature drops and the shock layer grows thinner. Also note the substantial influence of the ionization model on the O^+ fraction. This influence is less than 1% without electron-impact reactions (not shown in Fig. 12), whereas it is more than X_{N^+} with them.

In Fig. 13, mass loss rates obtained for the cases of equilibrium ablation, immobile adsorption with low activation energies, and mobile adsorption with high activation energies are shown. In these three calculations, reactions of ionization by electron impact are taken into account. To estimate the effect of these reactions, the case of equilibrium ablation without the reactions has been considered (clear squares). From Fig. 13 we see that immobile adsorption with low activation energies

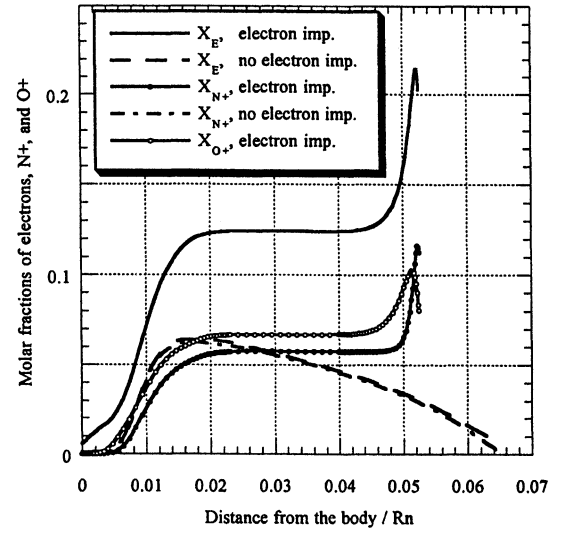

Fig. 12 Effect of ionization model on fractions of electrons and ions (equilibrium ablation, stagnation line).

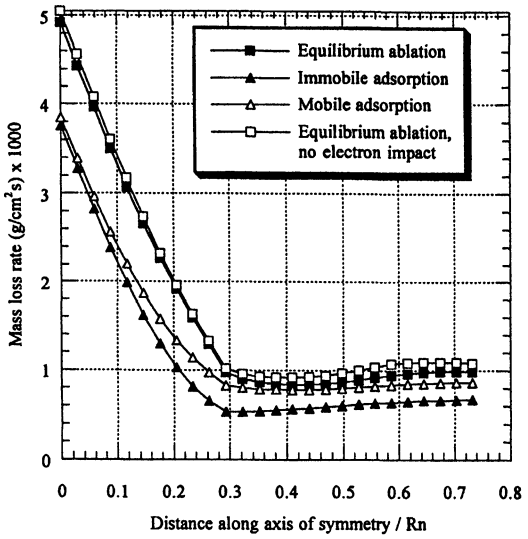

Fig. 13 Effect of ablation and ionization models on the mass loss rate.

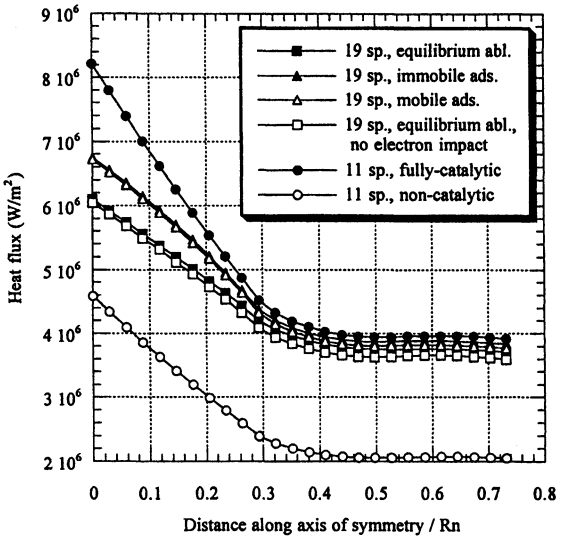

Fig. 14 Effect of ablation and ionization models on the heating rate.

may give a mass loss rate 1.6 times lower than mobile adsorption with high activation energies at the lateral part of the body. In the stagnation point, the difference is negligible, because sublimation processes dominate here (see trends of the plots at high tempertures in Fig. 3). The maximal effect of electron-impact ionization on the mass loss rate is about 10%.

In Fig. 14, the influence of ablation and ionization models on the heat flux are analyzed. Notations for calculations with ablation are the same as in Fig. 13. The limiting curves (with circles) are obtained for the 11-species airflows past the noncatalytic and fully catalytic (equilibrium) wall with electron-impact ionization taken into account. From Fig. 14 one can see that the effect of ablation on the heat flux is within 26% (compared with the fully catalytic calculations for the 11-species air). The effect of ablation model is within 11% (with respect to the heat flux for equilibrium ablation). The effect of the ionization model does not exceed 3%. Corresponding wall-temperature values are given in Fig. 15.

Shock standoff distances for the same cases are shown in Fig. 16. From the figure one can see that blowout leads to a slight increase of the layer thickness. Effects of catalycity and electron-impact ionization on the shock standoff distance are stronger. The first one is about 5% at the stagnation point and changes until it is 7.5% along the lateral part of the body, whereas the second one is about 20% at the stagnation point and drops until it is 2% at the body edge. The reason for the catalycity effect is the difference in the average mixture molar masses obtained for noncatalytic and fully catalytic walls and, consequently, in densities within the boundary layer. The reason for the ionization model effect is the difference in ion fractions.

The mass loss rate and the heat flux strongly depend on the equilibrium constants of sublimation–condensation processes, which in turn are related to the gas-phase equilibrium constants. Calculations in the case of equilibrium ablation with original (not corrected) Blottner's[20] data on C_3 dissociation give a stagnation-point mass loss rate that is 41% lower and a heat flux that is 20.5% higher than those shown in Figs. 13 and 14, respectively.

In Ref. 9, the aerodynamic flight environment for the MUSES-C re-entry capsule was analyzed throughout the entire re-entry flight path. They predicted the mass loss rate at the corresponding altitude as being 0.002 and 0.0035 g/cm²/s for noncatalytic and fully catalytic boundary conditions, respectively, whereas our results range from 0.0038 to 0.005 g/cm²/s

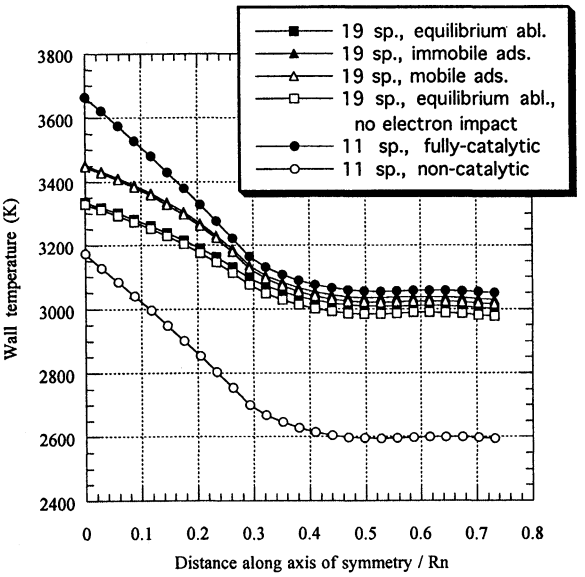

Fig. 15 Effect of ablation and ionization models on the wall temperature.

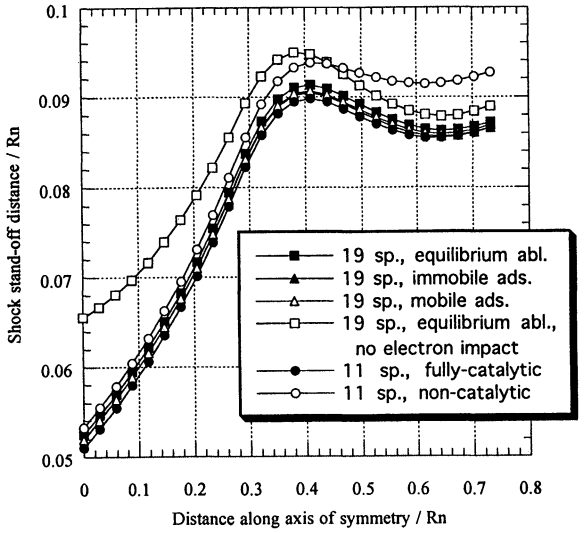

Fig. 16 Effect of ablation and ionization models on the shock standoff distance.

for the nonequilibrium ablation model and the equilibrium ablation model, respectively. Also in Ref. 19, the surface temperature is predicted as being 3000 and 3600 K for noncatalytic and fully catalytic boundary conditions, respectively. These values are comparable with our results. In Ref. 19, a traditional approach to implement the ablation chemistry including the evaporation was taken into account, whereas, in the present model, not only a carefully examined chemistry model is incorporated, but also a carefully chosen equilibrium constant is incorporated. The discrepancy in both the results is not significant, but the discrepancy itself is reasonable when we consider that the heat flux and the mass loss rate strongly depend on the equilibrium constants of sublimation–condensation processes, which in turn are related to the gas-phase equilibrium constants.

In all of the aforementioned calculations it is assumed that the mass production rates of ions at the wall equal zero. To estimate the effect of the wall catalycity with respect to charged particles, we specified equilibrium values of the ions fractions at the wall and calculated the heat fluxes to ablating and nonablating walls. It turned out that in this case the heat flux is only 1% higher than that in the case of the wall noncatalytic for ions. Obviously, this is a fairly general result, because strong deionization occurs in the boundary layer. At the same time one should be careful if the wall is cold. In this case equilibrium values of charged particles are becoming increasingly smaller, the Debye length grows, and the quasineutrality condition is violated. To bypass/solve the problem, it is necessary either to assume that the body surface is noncatalytic for ions or to solve the Poisson equation in the sheath.

Conclusions

A model for oxidation–sublimation processes on the carbonaceous surface of a re-entry vehicle is suggested. The model allows for the chemisorption of atomic oxygen and nitrogen, with the chemisorption of molecules and physisorption being neglected. The central ideas in the description of the kinetics are that the production rates of the absorbed species are zero (langmuir), and the equilibrium constants of all the heterogeneous and homogeneous reactions can be expressed via several independent ones. The model contains many empirical parameters, which should be selected from comparisons with experimental data. Three sets of the model input parameters can be recommended for estimations of the heating rates of ablating carbonaceous surfaces: two for mobile adsorption and one for immobile adsorption.

To estimate the effect of ablation on the re-entry capsule MUSES-C, VSL calculations have been carried out with different ablation models. Apparently, oxidation–sublimation of a surface close to pyrolytic graphite yields the minimal effect of ablation on the heating rate, whereas equilibrium ablation corresponds to the maximal drop of the heating rate because of ablation. This maximal drop is within 26%, compared with the calculations for the fully catalytic wall in the 11-species air, under the conditions discussed. The difference between the heating rates corresponding to ablation of a pyrolytic–graphite surface and equilibrium ablation is about 11%.

If the wall temperature is higher than 3000 K, the mass loss and heating rates strongly depend on the equilibrium constants of sublimation–condensation processes, which in turn depend on the gas-phase equilibrium constants. Therefore, to obtain physical results, the combined heterogeneous–homogeneous reaction system should account for the relationships between the constants. Mainly because of this, a previous prediction on the mass loss rate at the typical flight condition of the MUSES-C re-entry capsule shows a slight discrepancy with the present results.

The reactions of electron-impact ionization are important at $V_\infty > 10$ km/s under the conditions close to thermal equilibrium. The reactions affect the fractions of charged particles, which in turn affect temperature, which then affects the shock-layer thickness. All of these related effects may lead to a substantial change in radiation flux, which in a general case must be accounted for in the simulation of ablation phenomena.

Another important phenomenon, neglected in the present study for the sake of unambiguity of results, is thermal nonequilibrium. Apparently, one should solve corresponding equations for vibrational temperature(s) and for the energy of free electrons. Meanwhile, many models exist for $T - V$, $D - V$, $V - D$, $V - V$, $T - E$, $E - D$, and $E - V$ energy-exchange processes and coupling effects, and a separate study is necessary to create a definite thermochemical nonequilibrium model for the 19-species mixture.

References

[1]Kawaguchi, J., Fujiwara, A., and Sawai, S., "Sample and Return Mission from Asteroid Nereus via Solar Electric Propulsion," *Acta Astronautica*, Vol. 38, No. 2, 1996, pp. 87–101.

[2]Park, C., *Nonequilibrium Hypersonic Aerothermodynamics*, Wiley, New York, 1990.

[3]Park, C., "Effects of Atomic Oxygen on Graphite Ablation," *AIAA Journal*, Vol. 14, No. 11, 1976, pp. 1640–1642.

[4]Maahs, H. G., "Oxidation of Carbon at High Temperatures: Reaction-Rate Control or Transport Control," NASA TN D-6310, June 1971.

[5]Olander, D. R., Siekhaus, W., Jones, R., and Schwarz, J. A., "Reactiions of Modulated Molecular Beams with Pyrolytic Graphite. I. Oxidation of the Basal Plane," *Journal of Chemical Physics*, Vol. 57, No. 1, 1972, pp. 408–420.

[6]Olander, D. R., Jones, R. H., Schwarz, J. A., and Siekhaus, W. J., "Reactions of Modulated Molecular Beams with Pyrolytic Graphite. II. Oxidation of the Prism Plane," *Journal of Chemical Physics*, Vol. 57, No. 1, 1972, pp. 421–433.

[7]Blyholder, G., Binford, J. S., and Eyring, H., "A Kinetic Theory for the Oxidation of Carbonized Filaments," *Journal of Physical Chemistry*, Vol. 62, No. 3, 1958, pp. 263–267.

[8]Blyholder, G., and Eyring, H., "Kinetics of Graphite Oxidation," *Journal of Physical Chemistry*, Vol. 61, No. 5, 1957, pp. 682–688.

[9]Walker, P. L., Walker, R. L., Jr., Vastola, F. J., and Hart, R. J., "Oxygen-18 Tracer Studies on the Carbon-Oxygen Reaction," *Fundamentals of Gas-Surface Interactions*, edited by H. Saltsburg, J. N. Smith, and M. Rogers, Academic, New York, 1967, pp. 307–317.

[10]Spokes, G. N., and Benson, S. W., "Oxidation of a Thin Film of a Carbonaceous Char at Pressures Below 10 Torr," edited by H. Saltsburg, J. N. Smith, and M. Rogers, Academic, New York, 1967, pp. 318–328.

[11]Ong, J. N., Jr., "On the Kinetics of Oxidation of Graphite," *Carbon*, Vol. 2, No. 2, 1964, pp. 281–297.

[12]Scala, S. M., and Gilbert, L. M., "Sublimation of Graphite at Hypersonic Speeds," *AIAA Journal*, Vol. 3, No. 9, 1965, pp. 1635–1644.

[13]Kovalev, V. L., Suslov, O. N., and Tirskiy, G. A., "Phenomenological Theory for Heterogeneous Recombination of Partially Dissociated Air on High-Temperature Surfaces," *Molecular Physics and Hypersonic Flows*, edited by M. Capitelli, NATO ASI Series, Series C: Mathematical and Physical Sciences, Vol. 482, Kluwer, Boston, MA, 1996, pp. 193–201.

[14]Nasuti, F., Barbato, M., and Bruno, C., "Material-Dependent Catalytic Recombination Modeling for Hypersonic Flows," *Journal of Thermophysics and Heat Transfer*, Vol. 10, No. 1, 1996, pp. 131–136.

[15]Clark, A., *The Theory of Adsorption and Catalysis*, Academic, New York, 1970.

[16]Zhluktov, S. V., and Tirskiy, G. A., "An Effect of Vibration-Dissociation Coupling on the Heat Transfer and Aerodynamic Resistance in Hypersonic Flows past Blunt Bodies," *Izvestiya Akademii Nauk SSSR, Mekhanika Zhidkosti i Gaza*, Vol. 25, No. 3, 1990, pp. 141–151 (in Russian); also available in English in *Fluid Dynamics*, Vol. 25, No. 3, 1990, pp. 449–457.

[17]Zhluktov, S. V., Utyuzhnikov, S. V., and Tirskiy, G. A., "Numerical Investigation of Thermal and Chemical Nonequilibrium Flows past Slender Blunted Cones," *Journal of Thermophysics and Heat Transfer*, Vol. 10, No. 1, 1996, pp. 137–147.

[18]Zhluktov, S. V., Utyuzhnikov, S. V., and Abe, T., "Effect of the Surface Curvature Discontinuity on the Flowfield Around Spherically Blunted Cone," *Proceedings of the 2nd Asian Computational Fluid Dynamics Conference*, Vol. 2, Tokyo Univ., Tokyo, Japan, 1996, pp. 343–348.

[19]Suzuki, K., Kubota, H., Fujita, K., and Abe, T., "Chemical Nonequilibrium Ablation Analysis of MUSES-C Super-Orbital Reentry Capsule," AIAA Paper 97-2481, June 1997.
[20]Blottner, F. G., "Prediction of Electron Density in the Boundary Layer on Entry Vehicles with Ablation," NASA SP-252, Oct. 1970, pp. 219–240.
[21]Baker, R. L., "Graphite Sublimation Chemistry Nonequilibrium Effects," *AIAA Journal*, Vol. 15, No. 10, 1977, pp. 1391–1397.
[22]Goldstein, H. W., "The Reaction of Active Nitrogen with Graphite," *Journal of Physical Chemistry*, Vol. 68, No. 1, 1964, pp. 39–41.
[23]Walls, J. R., and Strickland-Constable, R. F., "Oxidation of Carbon Between 1000–2400°C," *Carbon*, Vol. 1, No. 3, 1964, pp. 333–338.
[24]Rosner, D. E., and Allendorf, H. D., "Comparative Studies of the Attack of Pyrolytic and Isotropic Graphite by Atomic and Molecular Oxygen at High Temperatures," *AIAA Journal*, Vol. 6, No. 4, 1968, pp. 650–654.
[25]Kang, S. W., and Dunn, M. G., "Theoretical and Experimental Studies of Reentry Plasmas," NASA CR-2232, April 1973.
[26]Bhutta, B. A., "A New Technique for the Computation of Severe Reentry Environments," AIAA Paper 96-1861, June 1996.
[27]Andriatis, A. V., Zhluktov, S. V., and Sokolova, I. A., "Transport Coefficients for Chemical Nonequilibrium Air Mixture," *Matamaticheskoe Modelirovanie*, Vol. 4, No. 1, 1992, pp. 44–64 (in Russian).
[28]Balakrishnan, A., "Correlations for Specific Heats of Air Species to 50,000 K," AIAA Paper 86-1277, June 1986.
[29]Tirskii, G. A., Utyuzhnikov, S. V., and Yamaleev, N. K., "Efficient Numerical Method for Simulation of Supersonic Viscous Flow past a Blunted Body at a Small Angle of Attack," *Computers and Fluids Journal*, Vol. 23, No. 1, 1994, pp. 103–114.